

Article

Numerical Study on Flow and Heat Transfer Characteristics of Supercritical CO₂ in Zigzag Microchannels

Yi Tu¹ and Yu Zeng^{2,*} 

¹ School of Mechanical Engineering, Hunan University of Arts and Science, Changde 415000, China; tuyi.huas@outlook.com

² School of Aeronautic Science and Engineering, Beihang University, Beijing 100191, China

* Correspondence: zengyu@buaa.edu.cn; Tel.: +86-186-1840-5545

Abstract: The zigzag channel is the uppermost channel type of an industrial printed circuit heat exchanger (PCHE). The effect of geometric properties on the flow and heat transfer performance of the channel is significant to the PCHE design and optimization. Numerical investigations were conducted on the flow and heat transfer characteristics of supercritical CO₂ (sCO₂) in semicircular zigzag channels by computational fluid dynamics method. The shear stress transfer (SST) $k-\omega$ model was used as turbulence model and the National Institute of Standards and Technology (NIST) real gas model with REFPROP database was used to evaluate the thermophysical parameters of sCO₂ in this numerical method. The effectiveness of the simulation method is verified by experimental data. Thermal hydraulic performance for zigzag channels with different pitch lengths, bending angles, and hydraulic diameters are studied comparatively based on this numerical method, with the boundary conditions which cover the pseudocritical point. The comparison results show that reducing the bending angle and pitch length will strengthen the effect of boundary layer separation on the leeward side of the wall and enhance the heat transfer performance, but the pressure drop of the channel will also increase, and the decrease of channel hydraulic diameter is beneficial to the heat transfer enhancement, but it is not as significant as that of the straight channel.

Keywords: supercritical CO₂; zigzag channel; micro channel; heat transfer; computational fluid dynamics



Citation: Tu, Y.; Zeng, Y. Numerical Study on Flow and Heat Transfer Characteristics of Supercritical CO₂ in Zigzag Microchannels. *Energies* **2022**, *15*, 2099. <https://doi.org/10.3390/en15062099>

Academic Editors: Abderrahmane Bâiri, Angel A. Juan and Marcin Kamiński

Received: 10 February 2022

Accepted: 11 March 2022

Published: 13 March 2022

Publisher's Note: MDPI stays neutral with regard to jurisdictional claims in published maps and institutional affiliations.



Copyright: © 2022 by the authors. Licensee MDPI, Basel, Switzerland. This article is an open access article distributed under the terms and conditions of the Creative Commons Attribution (CC BY) license (<https://creativecommons.org/licenses/by/4.0/>).

1. Introduction

A printed circuit heat exchanger (PCHE) is a type of compact heat exchanger with high efficiency, high application pressure, and high application temperature. It was invented in Australia in 1980 and promoted for commercial application by Heatric. It has broad application prospects in the fields of ultra-high-temperature gas-cooled reactors, floating liquefied natural gas storage units, and other industrial energy [1]. PCHE typically employs diffusion-bonded arrays of plates where microchannels are formed by chemical etching [2]. The typical cross section shape is semicircular and the hydraulic diameter in a PCHE passage is between 700 μm and 1.5 mm [3]. The flow channel geometries can be designed as straight, zigzag, S-shape, and airfoil-finned channels [4]. However, the zigzag-type channel is more widely used in industrial applications. CO₂ is a nontoxic and inexpensive gas. It has excellent thermophysical properties (high specific heat, high thermal conductivity, and low viscosity) near the pseudocritical point, as shown in Figure 1, which can considerably enhance the heat transfer without sacrificing the hydraulic performance [5]. Consequently, the application of CO₂ in PCHE has become the focus of researchers.

Heat transfer and hydraulic characteristics are the basis of PCHE thermal design. Various experimental and numerical investigations have been performed to optimize the channel structures, fluid mediums, and operation conditions. Nikitin and his team first published the experimental results of the flow and heat transfer characteristics of sCO₂ in zigzag PCHE in 2016 and developed the correlations of Nu and f , while the correlations

are only applicable to channels of the specific geometric parameters and Reynolds number range of those used in the experimental study [6]. Kruiuzenga et al. investigated the thermal–hydraulic performance of $s\text{CO}_2$ in a straight channel with semicircular cross section using both experimental and numerical methods, the analysis results showed that the commercial computational fluid dynamics (CFD) software can well predict the internal heat transfer characteristics of the PCHE channel [7]. Saeed and Kim also conducted the numerical analysis of an $s\text{CO}_2$ PCHE using ANSYS-CFX and validated the simulation results using published experimental data [8]. Tu and Zeng studied the flow and heat transfer performance in semicircular straight channels of $s\text{CO}_2$ fluid for both cooling and heating process using CFD method. A modified model based on Douglas A. Olson [9] correlation was proposed to predict the heat transfer performance of $s\text{CO}_2$ in semicircular channels for both heating and cooling conditions [10]. These literature conclusions fully confirm the feasibility of the numerical method.

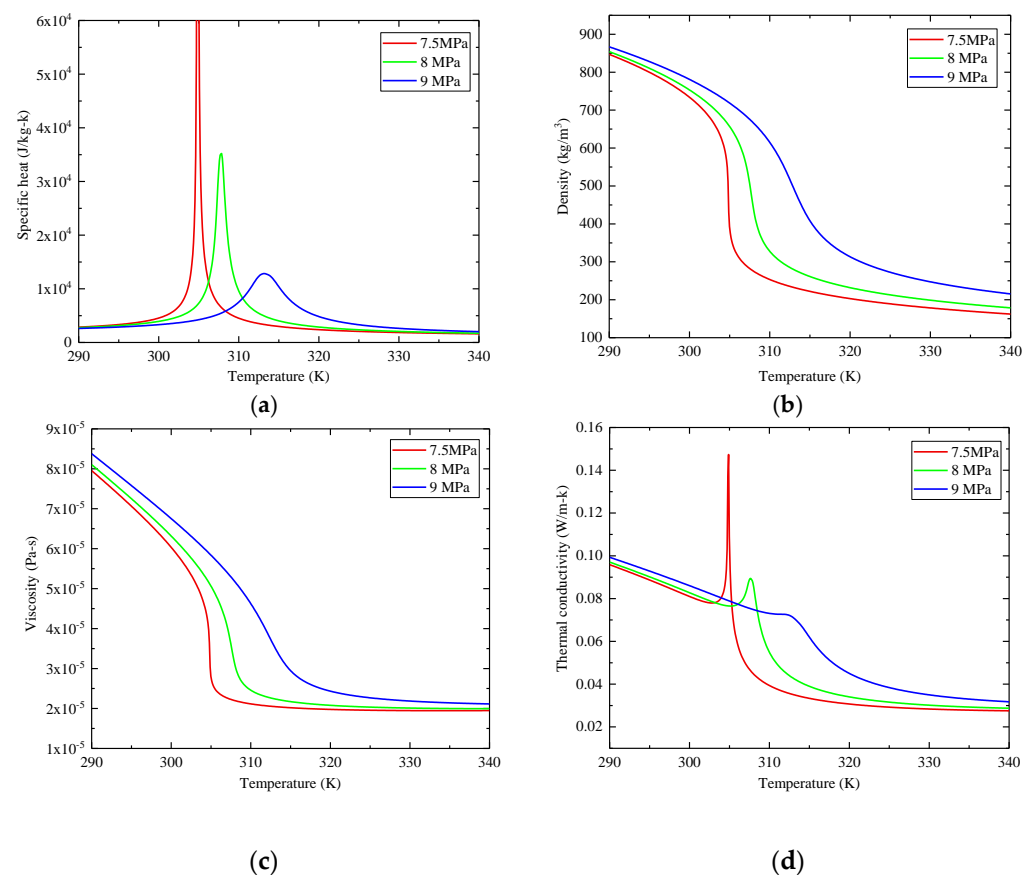


Figure 1. Thermophysical properties of supercritical CO₂ at different pressure: (a) specific heat; (b) density; (c) dynamic viscosity; (d) thermal conductivity.

Subsequently, a large number of studies focused on finding better channel types. Kim et al. compared the heat transfer and hydraulic performance of $s\text{CO}_2$ in PCHE with zigzag and airfoil-shaped fins. It was found that the thermal performance of the airfoil fin was close to that of zigzag, but the airfoil fin had lower pressure loss [11]. Mohammed et al. investigated the effect of channel shapes (zigzag, curve, and step) on the thermal and hydraulic performance of PCHE and found that the zigzag channels have the highest value of heat transfer coefficient and pressure drop [12]. Matsuo et al. conducted numerical simulations of three different channel types (zigzag, chamfered zigzag, airfoil) to study the geometrical effects on the local heat transfer coefficient and pressure drop for supercritical CO₂ in PCHE and developed new correlations for Nu of the zigzag channels [13]. In the research of [14–16], the PCHE with zigzag channel and discontinuous S-shaped fins were

numerically and experimentally investigated, and it was found that the S-shaped channel can significantly improve the hydraulic performance while keeping almost equal heat transfer performance compared to the zigzag channels.

There are also studies focusing on thermal hydraulic characteristics of the other fluid media in PCHE channels. Dai et al. studied the flow and heat transfer performance of water in the semicircular zigzag passage experimentally [17]. Minghui Chen et al. investigated the thermal–hydraulic performance of a zigzag channel PCHE using helium as fluid media [18].

Most of the studies on the flow and heat transfer characteristics of PCHE channels use a specific geometric parameter channel or straight channel, or the comparison between zigzag channel and other types of channels such as S-type and discontinuous airfoil fin type. The experimental data and empirical correlations given in these studies are also limited to a certain type of channel, and the operating pressure, fluid bulk temperature, and Reynolds number are limited to a certain range. However, there are few studies on the effect of geometric parameters on the flow and heat transfer performance of a zigzag channel. This paper aims at modeling the forced convection heat transfer of CO₂ within the zigzag channels, which are the main channel type of PCHE, and studies the effects of its main geometric parameters (hydraulic diameter, pitch length, and bending angle) on its internal flow and heat transfer parameters, especially near the pseudocritical point. The numerical method and analysis results of this study can be used as a reference for PCHE industrial design and channel performance investigation.

2. Numerical Modeling

A numerical method for analyzing the steady-state flow and heat transfer properties of a zigzag channel is defined. In this method, ANSYS Fluent 2019 is used to solve the governing equations of the steady turbulent flow of sCO₂ in the zigzag channels. The NIST real gas model with REFPROP V9.1 database was used to evaluate the thermodynamics and transport of approximately of CO₂. Yoon et al. [19] and Ren et al. [20] conducted comparative studies using STD k– ϵ , realizable k– ϵ , and SST (shear stress transport) k– ω turbulence models to simulate the thermal–hydraulic performance of sCO₂ intube-flowing and found that the SST k– ω turbulence model gives the best quantitative prediction. The same conclusion was likewise reached in [21–24]. Therefore, the SST k– ω model is adopted for further analysis in this study. The pressure-based coupled algorithm was used to establish the coupling of velocity and pressure. The numerical simulation is considered convergent as all iterative residuals of the governing equations are less than 10^{−5}, and area-weighted average outlet temperature and area-weighted average inlet pressure are stable.

2.1. Geometry and Boundary Conditions

The flow and heat transfer performance of CO₂ in horizontal zigzag channels is investigated in this paper. Figure 2 shows a schematic diagram of the computational domain with the boundary condition adopted in this research. The study will consider the effects of different geometric factors, including hydraulic diameter, bending angle, and pitch length on the internal flow and heat transfer characteristics of the channel, as shown in Table 1. To check the independent effect of the geometric parameter, the comparative study only changes one geometric parameter at a time, and the rest remains unchanged. For example, for investigating the effect of bend angle θ on the channel flow and heat transfer performance, four types of bend angle, 100°, 115°, 140°, and 180° (straight), are considered for the geometric model, while L_p is fixed to 7.75 mm and d_h is fixed to 2 mm.

As shown in Table 2, the inlet temperature was changed from 280 K to 350 K to ensure the bulk temperature T_b covers the pseudocritical point of CO₂ for this analysis. The outlet pressure of CO₂ varies between 7.5 MPa and 9 MPa to keep its condition near the pseudocritical point. Constant wall heat flux (12 kW/m² for heating case and −12 kW/m² for cooling case) and mass flux 200 kg/m²-s were adopted in this numerical simulation. The thermal properties of CO₂ were obtained from NIST Database (REFPROP V9.1).

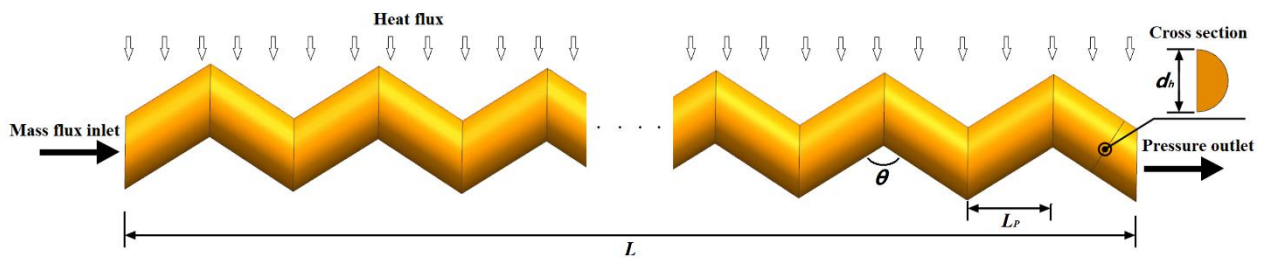


Figure 2. Physical model of zigzag channel.

Table 1. Geometric parameters.

Geometric Parameters	Values
Channel hydraulic diameters, d_h , mm	1.17 (experimental validation), 2, 4
Bending angle, θ , °	100, 115, 140, Straight
Channel pitch length, L_p , mm	3, 4.5, 6, 7.75
Channel total length, L , mm	500

Table 2. Boundary conditions in detail.

Inlet		Outlet	Wall
Temperature (K)	Mass flux ($\text{kg}/\text{m}^2\text{-s}$)	Pressure (MPa)	Constant heat flux (kW/m^2)
280–350	200	7.5, 8, 9	± 12

2.2. Governing Equations

The governing equations regarding the continuity, momentum, and energy are expressed as Equations (1)–(3).

- (1) Continuity equation:

$$\frac{\partial}{\partial x_i} (\rho u_i) = 0 \quad (1)$$

- (2) Momentum equation [25]:

$$\frac{\partial}{\partial x_j} (\rho u_i u_j) = -\frac{\partial p}{\partial x_i} + \frac{\partial \tau_{ij}}{\partial x_j} + \rho g_i \quad (2)$$

- (3) Energy equation:

$$\frac{\partial}{\partial x_i} (u_i (\rho E + p)) = \frac{\partial}{\partial x_i} \left(k_{eff} \frac{\partial T}{\partial x_i} \right) \quad (3)$$

where ρg_i is the gravitational body force, u_i is overall velocity vector, T is the temperature, ρ is the density, u_i is the velocity vector, E is the total energy, p is the static pressure, τ_{ij} is the stress tensor, and k_{eff} is the effective conductivity ($k_{eff} = k + k_t$, k_t is the turbulent thermal conductivity).

- (4) Direct numerical simulation (DNS) of Navier–Stokes equations is the most accurate method for turbulence; however, it is not feasible in most situations to resolve the wide range of scales in time and space as the CPU requirements by far exceed the existing capacity. For this reason, averaging procedures such as the Reynolds method have to be applied to the Navier–Stokes equations to filter out the turbulent spectrum [26]. However, the averaging process introduces additional unknown terms into the transport equations that need to be provided by suitable turbulence models. The SST k – ω turbulence model is used in this paper and is described as follows.

The transport equations of the k - ω model are expressed as Equations (4) and (5):

$$\frac{\partial}{\partial x_i}(\rho k u_i) = \frac{\partial}{\partial x_j} \left(\Gamma_k \frac{\partial k}{\partial x_j} \right) + G_k - \rho \beta^* k \omega \quad (4)$$

$$\frac{\partial}{\partial x_i}(\rho \omega u_i) = \frac{\partial}{\partial x_j} \left(\Gamma_\omega \frac{\partial \omega}{\partial x_j} \right) + G_\omega - \rho \beta \omega^2 \quad (5)$$

where G_k is the generation of turbulence kinetic energy k due to mean velocity gradients, G_ω is the generation of ω , and Γ_k and Γ_ω represent the effective diffusivity of k and ω calculated by Equations (6) and (7).

$$\Gamma_k = \mu + \mu_t \left(\frac{F_1}{\sigma_{k1}} + \frac{1 - F_1}{\sigma_{k2}} \right) \quad (6)$$

$$\Gamma_\omega = \mu + \mu_t \left(\frac{F_1}{\sigma_{\omega1}} + \frac{1 - F_1}{\sigma_{\omega2}} \right) \quad (7)$$

where σ_k and σ_ω are turbulent Prandtl numbers for k and ω , respectively, μ is the dynamic viscosity of the fluid, and F_1 is calculated as Equations (8)–(10).

$$F_1 = \tanh(\phi_1^4) \quad (8)$$

$$\phi_1 = \min \left[\max \left(\frac{\sqrt{k}}{0.09 \omega y}, \frac{500 \mu}{\rho y^2 \omega} \right), \frac{4 \rho k}{\sigma_{\omega 2} D_\omega y^2} \right] \quad (9)$$

$$D_\omega = 2(1 - F_1) \rho \sigma_{\omega 2} \frac{1}{\omega} \frac{\partial k}{\partial x_j} \frac{\partial \omega}{\partial x_j} \quad (10)$$

The turbulent viscosity μ_t of the SST $k\omega$ model is calculated using Equations (11)–(15).

$$\mu_t = \frac{\rho k}{\omega} \frac{1}{\max \left(\frac{1}{a^*}, \frac{\sqrt{2 S_{ij} F_2}}{a_1 \omega} \right)} \quad (11)$$

$$S_{ij} = \frac{1}{2} \left(\frac{\partial u_i}{\partial x_j} + \frac{\partial u_j}{\partial x_i} \right) \quad (12)$$

$$F_2 = \tanh(\phi_2^2) \quad (13)$$

$$\phi_2 = \max \left(2 \frac{\sqrt{k}}{0.09 \omega y}, \frac{500 \mu}{\rho y^2 \omega} \right) \quad (14)$$

$$a^* = a_\infty^* \left(\frac{a_0^* + \frac{\rho k}{6 \mu \omega}}{1 + \frac{\rho k}{6 \mu \omega}} \right) \quad (15)$$

where μ_t is the turbulent viscosity, y is the wall distance, and the constants used in the SST model are as follows: $a_\infty^* = 1$, $a_1 = 0.31$, $\sigma_{k1} = 1.176$, $\sigma_{k2} = 1$, $\sigma_{\omega 1} = 2$, $\sigma_{\omega 2} = 1.168$, $a_0^* = 0.024$.

The second-order upwind scheme of Equation (16) is used to discretize the convective term of the above governing Equation [27].

$$\varphi_{f,sou} = \varphi + \nabla \varphi \cdot \vec{r} \quad (16)$$

where φ and $\nabla \varphi$ are the cell-centered value and its gradient in the upstream cell and \vec{r} is the displacement vector from upstream cell centroid to the face centroid.

2.3. Data Reduction

The hydraulic diameter, d_h , was defined as Equation (17):

$$d_h = \frac{4A}{C_{wet}} \quad (17)$$

where A is the semicircular cross section area of the channel, and C_{wet} is the wet circumference of the cross section.

The average heat convection coefficient, h , was defined as Equation (18):

$$h = \frac{Q_w}{T_w - T_b} \quad (18)$$

where Q_w is the heat flux of the wall, T_w is the average wall temperature, and T_b is the fluid bulk temperature.

The channel total pressure drop, ΔP , was defined as Equation (19):

$$\Delta P = P_{in} - P_{out} \quad (19)$$

where P_{in} and P_{out} are area-weighted average pressure at the inlet and outlet of the channel, respectively.

2.4. Grid Independence and Model Validation

Meshes in this study are generated using ICEM CFD 2019, and the size of the first layer adjacent to the wall is less than 2×10^{-6} m to keep the wall $y^+ < 1$. Structured hexahedral cells are used in the whole computational domain, and the mesh is locally densified at the bend of the flow direction, as illustrated in Figure 3.

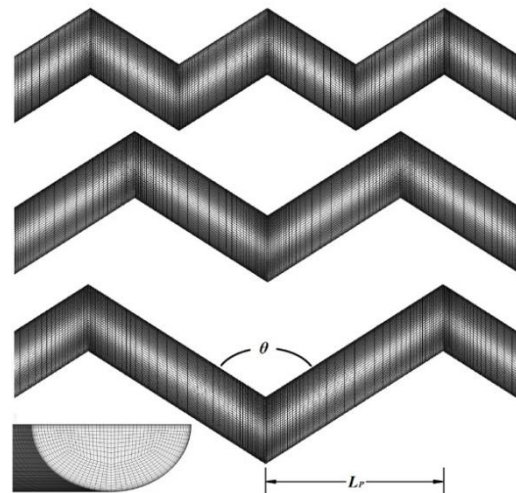


Figure 3. Mesh structure of the computational domain.

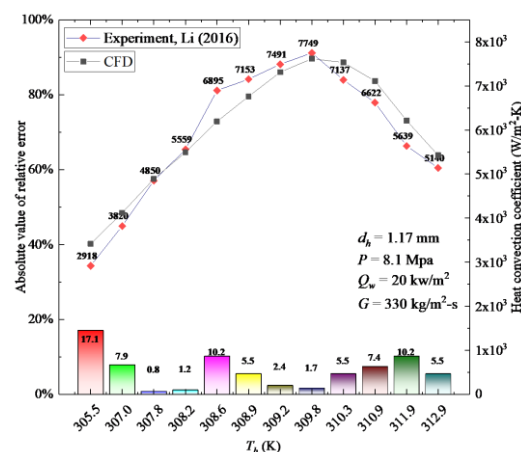
Mesh independence analysis was performed with five different mesh sizes of 91,656, 152,988, 233,508, 314,028, and 394,548. Percentage changes in physical variables h and ΔP were chosen as the basis for independence judgment. As the comparison result listed in Table 3, the relative error percentage of h changes from 11.01% to 1.17%, and the relative error percentage of ΔP changes from 19.78% to 0.59% with the mesh refinement. Consequently, the mesh size of 314,028 elements is considered sufficient, and 300,000 is used as the baseline for all the rest of the simulations.

Table 3. Mesh independence analysis.

No.	Number of Elements	h (W/m ² -K)	Error (%)	ΔP (Pa)	Error (%)
1	91,656	1655.298	11.01%	629.7	19.78%
2	152,988	1644.926	11.56%	639.9	21.72%
3	233,508	1737.778	6.57%	605.9	15.26%
4	314,028	1838.227	1.17%	528.8	0.59%
5	394,548	1860.027	0.00%	525.7	0.00%

2.5. Validation by Experimental Data

The experimental data in [28] were used to verify the accuracy of the numerical method. The experiments were carried out to investigate the thermal performance of sCO₂ in a straight channel with semicircular cross section. The hydraulic diameter and total length of the channel are 1.17 mm and 500 mm. The operating pressure, heat flux, and mass flux are 8.1 MPa, -20 kW/m^2 , and $330 \text{ kg/m}^2\text{-s}$, respectively. As shown in Figure 4, the CFD simulation results and experimental data maintain a good consistency with the maximum relative error 17.1% over all analyzed T_b range, which covers the pseudocritical point. Thus, the numerical method adopted in this study for the flow and heat transfer performance of sCO₂ in the semicircular channel is reliable and comparatively accurate.

**Figure 4.** Validation with experimental data [28].

3. Results and Discussion

3.1. Effect of L_p on the Channel Flow and Heat Transfer Performance

To study the effect of L_p on thermal and hydraulic performance of zigzag channel, three different L_p (3, 4.5, and 6 mm) are considered for this comparative study. The other geometric factors d_h and θ take the value 1.17 mm and 115° , respectively, and remain unchanged to avoid coupling effects. The channel has an inlet mass flux of $G = 200 \text{ kg/m}^2\text{-s}$, an outlet pressure of $P_{out} = 8 \text{ MPa}$, and a wall heat flux of $Q_w = \pm 12 \text{ kW/m}^2\text{-k}$. The bulk temperature T_b of CO₂ varies between 280 K and 360 K, covering the pseudocritical temperature T_m .

As shown in Figure 5, h of the three channels gradually increases and reaches the maximum value as the T_b of the fluid approaches T_m . This is due to the surge of the specific heat and thermal conductivity of CO₂ near the pseudocritical point. ΔP of the three types of channels decrease with the increase of T_b . This is mainly because the density of CO₂ decreases with the rising of T_b . It can be seen from the comparison results of the three channels that the heat convection coefficient h and pressure drop ΔP both decrease with the rising L_p .

Figure 6 shows the velocity vector along the zigzag channel with different L_p . The flow-field distribution possesses certain periodicity. A large velocity gradient occurs at the

channel corner and the maximum velocity in the channel also appears in this area. Boundary layer separation occurs at the corner of the channel and the local velocity increases due to the appearance of vortex. As the velocity direction is different from the wall direction of the next pitch, it can strengthen the mixing of the mainstream and the fluid near the wall, which is conducive to the heat transfer enhancement. As can be seen from the partial enlarged view, the local velocity increases with the reduction of channel L_p , which means that the fluid at the boundary region is mixed with the fluid in the core region more sufficiently. As a result, the reduction of L_p enhances the channel heat transfer, and improves the channel total heat convection coefficient h . The local flow resistance ΔP also rises with the reduction of L_p as the wall separation increases.

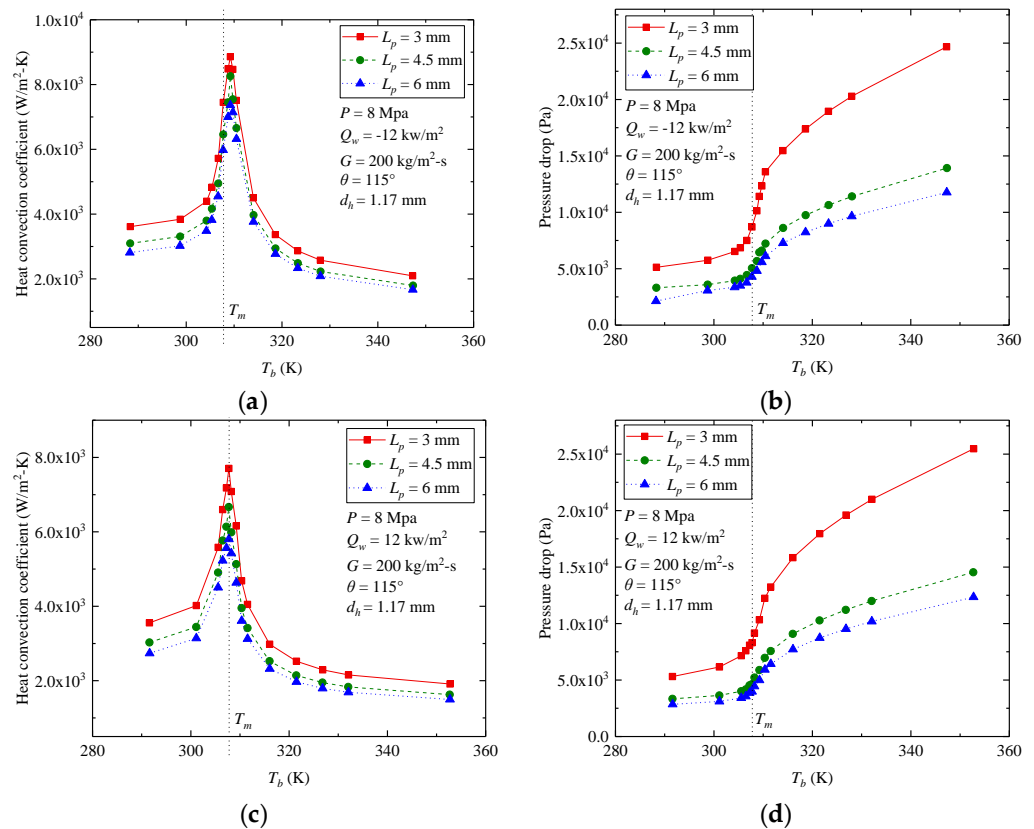


Figure 5. Effect of L_p on flow and heat transfer performance: (a) h of cooling case; (b) ΔP of cooling case; (c) h of heating case; (d) ΔP of heating case.

Figure 7 represents the local convective heat transfer coefficient in zigzag channel with different L_p . The local heat transfer coefficient increases significantly on the windward side of the corner area. It is because the boundary layer is locally thinner under the direct flushing of the incoming flow. As mentioned above, the local fluid velocity increases with the decrease of channel L_p , which also leads to the local heat transfer coefficient increasing.

3.2. Effect of θ on the Channel Flow and Heat Transfer Performance

In this part of the analysis, four different θ of the channel (100° , 115° , 140° , and straight) are considered for this comparative study with the inlet mass flux $G = 200 \text{ kg/m}^2\text{-s}$, outlet pressure $P_{out} = 8 \text{ MPa}$, and wall heat flux $Q_w = \pm 12 \text{ kw/m}^2\text{-k}$. d_h and L_p of the channels remain unchanged with the values 2 mm and 7.75 mm, respectively. The bulk temperature T_b of the CO_2 varies between 280 K and 360 K to cover the pseudocritical temperature T_m .

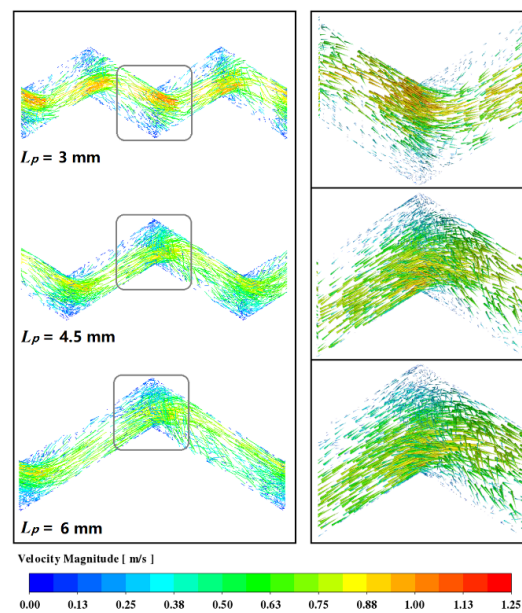


Figure 6. Velocity vector along the zigzag channel with L_p of 3 mm, 4.5 mm, and 6 mm.

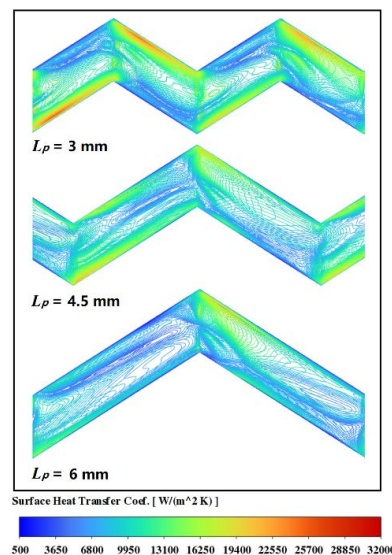


Figure 7. Local heat transfer coefficient of the zigzag channel with L_p of 3 mm, 4.5 mm, and 6 mm.

As can be seen from Figure 8, h and ΔP both decrease with the increase of θ , and better thermal performance for all of the zigzag channels is demonstrated, compared with the straight channel. The variation trend of h and ΔP of zigzag channel with T_b is the same as that of the straight channel. This provides an approach for defining the flow and heat transfer correlations in zigzag channels, as there have been several studies on the correlations of Nu of the sCO_2 semicircular straight channel [29,30].

Figure 9 shows the comparison of the velocity vector along the channel with different bend angles of the zigzag channel. A sharper bending angle will significantly increase the local fluid velocity at the turning position and aggravate the separation of the boundary layer, which will result in more violent mixing of fluid between the wall area and the core region. It means that the decrease of θ enhances the channel convective heat transfer under the geometric parameters of the current study. Therefore, h increases with the decrease of θ . As $\theta = 180^\circ$, the channel becomes a straight channel, and h is smaller than any of the zigzag channels with bending angles.

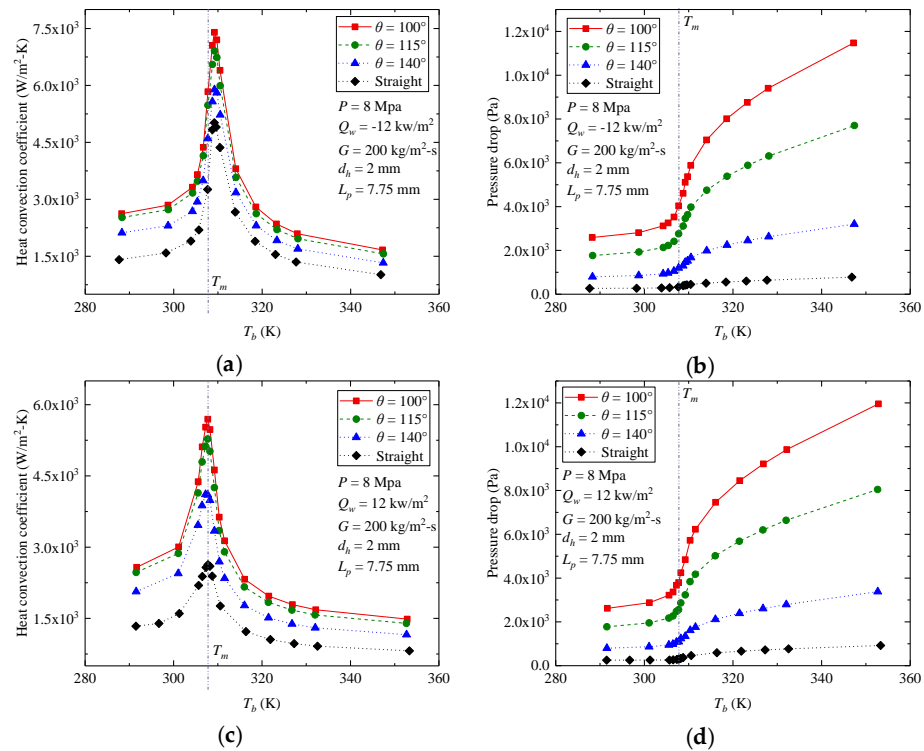


Figure 8. Effect of θ on flow and heat transfer performance: (a) h of cooling case; (b) ΔP of cooling case; (c) h of heating case; (d) ΔP of heating case.

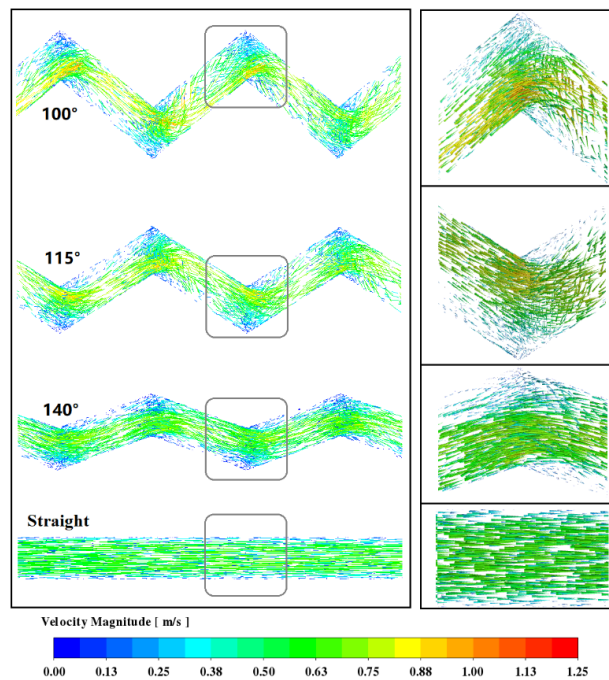


Figure 9. Velocity vector along the zigzag channel with θ of 100° , 115° , 140° , and straight.

Figure 10 shows the contour plots of local convective heat transfer coefficient in zigzag channel under different θ . It can be seen that the convective heat transfer coefficient of the wall surface of the zigzag channel is significantly higher than that of the straight channel. The region with the highest local convective heat transfer coefficient appears on the windward side of the turning angle of zigzag channel. It is because this area is washed by the mainstream and has a locally thinner boundary layer.

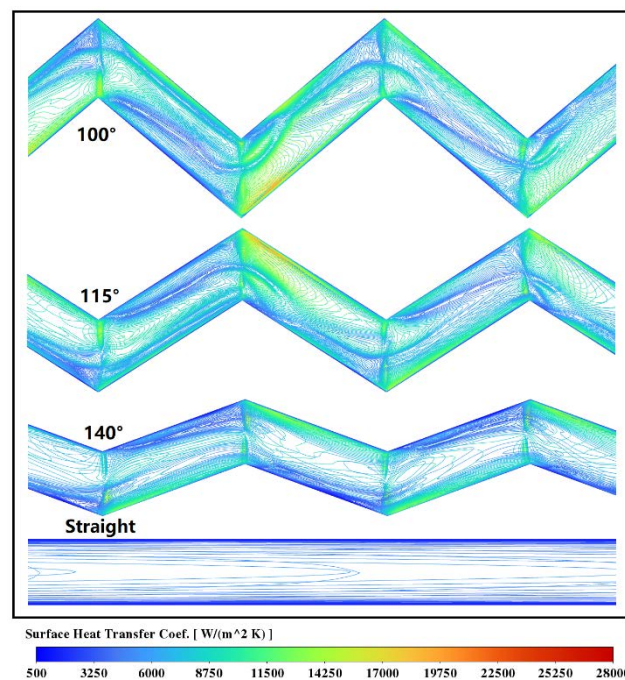


Figure 10. Local heat transfer coefficient of the zigzag channel with θ of 100° , 115° , 140° , and straight.

3.3. Effect of d_h on the Channel Flow and Heat Transfer Performance

In this comparative evaluation study, three different d_h of 1.17, 2, and 4 mm are used. The other geometric factors L_p and θ are set to 4.5 mm and 115° , respectively and remain unchanged. The channel has an inlet mass flux of $G = 200 \text{ kg/m}^2\text{-s}$, an outlet pressure of $P_{out} = 8 \text{ MPa}$, and a wall heat flux of $Q_w = \pm 12 \text{ kw/m}^2\text{-k}$. The bulk temperature T_b of CO_2 varies between 280 K and 360 K, covering the pseudocritical temperature T_m .

With the reduction of channel d_h , the distance from the mainstream region to the wall also decreases, which is theoretically conducive to the heat transfer performance, and there are indeed such conclusions in the study on the thermal performance of the straight channel in [24,31]. Nonetheless, for the zigzag channels, the heat convection coefficient h does not show an obvious increasing trend with the decrease of d_h . It can be seen from Figure 11 that h and ΔP increase significantly as d_h changes from 4 mm to 2 mm, especially in the heating cases. However, when d_h changes from 2 mm to 1.17 mm, neither h nor ΔP show significant change. This is different from the conclusion in the semicircular straight channel study.

Through the previous analysis cases, we found that the separation of boundary layer promotes the mixing and diffusion in the fluid and enhances the heat transfer performance of the zigzag channel. However, on the other hand, it will also reduce the effective heat transfer area of the wall, which is disadvantageous to the heat exchange. Figure 12 shows us another possible scenario. As for the $d_h = 4 \text{ mm}$ diameter case, the boundary layer separation area accounts for a large proportion of the total heat exchange area and the weakening effect of the separation of boundary layer on heat transfer becomes dominant. It can also be seen from Figure 13 that the local heat convective coefficient of the $d_h = 4 \text{ mm}$ channel has not been obviously enhanced on the windward side compared to the $d_h = 1.17 \text{ mm}$ and $d_h = 2 \text{ mm}$ channels.

As can be also seen from Figure 12, the boundary layer separation effect is weakened with the decrease of the d_h . In the $d_h = 1.17 \text{ mm}$ and $d_h = 2 \text{ mm}$ diameter cases, the boundary layer separation area will not account for as large a proportion of the total wall area as that presented in $d_h = 4 \text{ mm}$ case, which means that the boundary layer separation has a positive effect on the heat transfer performance of the 1.17 mm and 2 mm channels. When $L_p \gg d_h$, this positive effect is enhanced with the increase of d_h . At the same time, there is an opposite influence whereby the heat transfer will be weakened with the increase of d_h due to the increasing distance between mainstream region and the wall. The combination

of these two effects makes the convective heat transfer coefficient close for the 1.17 mm and 2 mm channels.

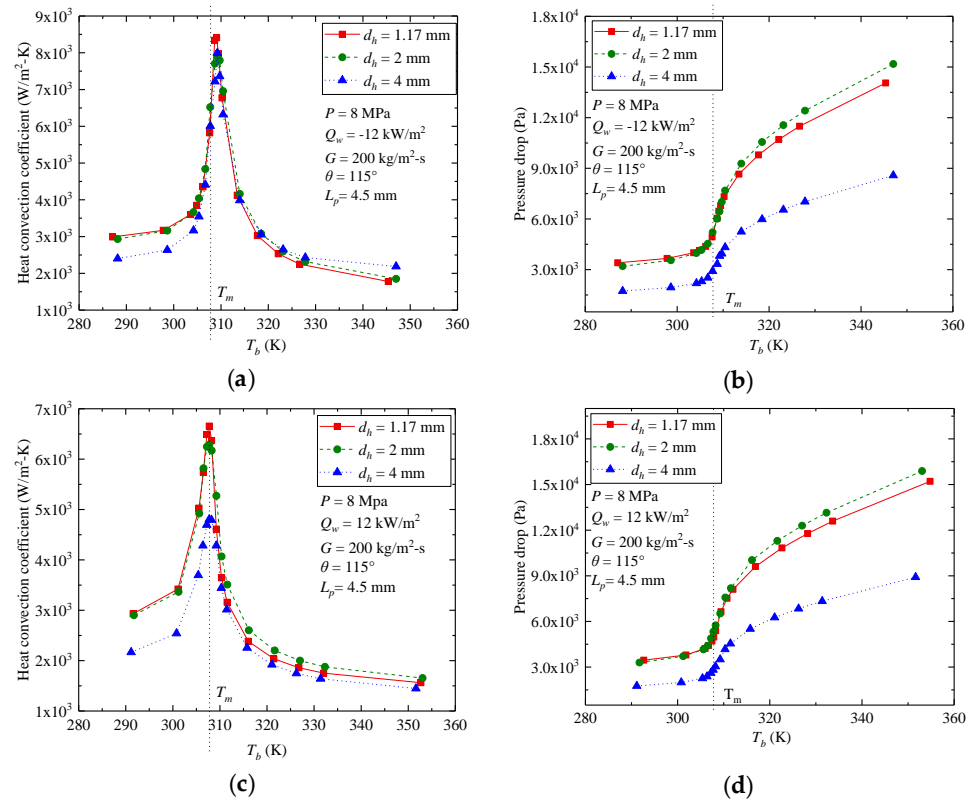


Figure 11. Effect of d_h on flow and heat transfer performance: (a) h of cooling case; (b) ΔP of cooling case; (c) h of heating case; (d) ΔP of heating case.

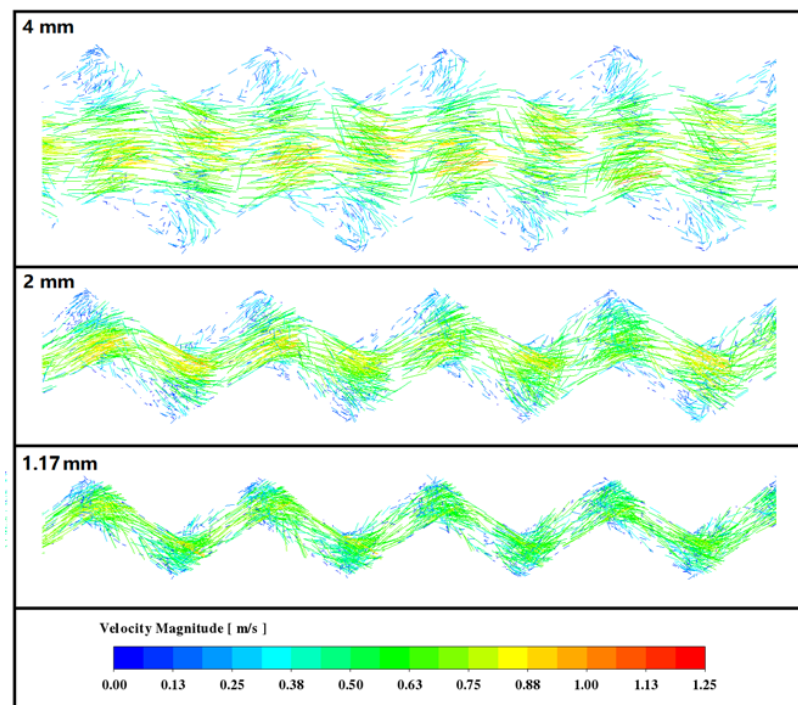


Figure 12. Velocity vector along the zigzag channel with d_h of 1.17 mm, 2 mm, and 4 mm.

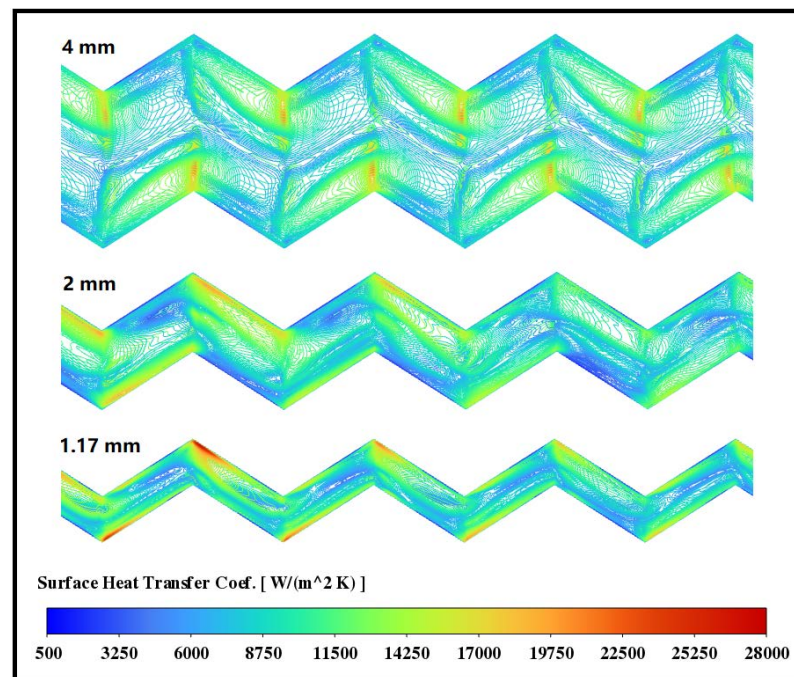


Figure 13. Local heat transfer coefficient of the zigzag channel with d_h of 1.17 mm, 2 mm, and 4 mm.

All three geometric parameters produce effects on the flow and heat transfer performance of the zigzag channel and have a certain regularity. When the size of d_h is close to L_p , the wall separation caused by channel turning will not strengthen the heat transfer performance. For industrial design, from the point of view of enhancing heat transfer, the L_p should be significantly larger than d_h for the zigzag channels.

4. Conclusions

The thermal and hydraulic performance of $s\text{CO}_2$ in zigzag channels of different pitch lengths (3 mm, 4.5 mm, 6 mm, 7.75 mm), bending angles (100° , 115° , 140° , straight), and hydraulic diameters (1.17 mm, 2 mm, 4 mm) are studied comparatively with the boundary condition covering the pseudocritical point using the CFD method. In this numerical method, the SST $k-\omega$ is adopted as the turbulence model and shows the quantitative prediction of the experiments' heat transfer data. The following conclusions were obtained:

- (1) The drastic change of CO_2 thermophysical parameters has a significant effect on the hydraulic and heat transfer characteristics of the zigzag channel near the pseudocritical point, and its variation tendency with bulk temperature is the same as that of the straight channel.
- (2) The reduction of pitch length enhances the effect of boundary layer separation behind the corner, which can improve the heat transfer performance. As a result, the heat convective coefficient and pressure drop of $s\text{CO}_2$ in the zigzag channel increase with the decrease of the pitch length.
- (3) The decrease of channel bend angle can also increase the local velocity at the turning location and enhance the boundary layer separation effect. Therefore, the heat convective coefficient and pressure drop of $s\text{CO}_2$ in the zigzag channel both increase with the decrease of channel bend angle.
- (4) The decrease of channel hydraulic diameter is conducive to the heat transfer of the zigzag channel, but it is not as significant as that of the straight channel, because the boundary layer separation effect will be weakened with the decrease of channel hydraulic diameter.

Author Contributions: Conceptualization, Y.T. and Y.Z.; methodology, Y.T.; software, Y.T.; validation, Y.T. and Y.Z.; formal analysis, Y.T.; investigation, Y.T.; resources, Y.Z.; data curation, Y.T.; writing—original draft preparation, Y.T.; writing—review and editing, Y.Z.; visualization, Y.T.; supervision, Y.Z.; project administration, Y.T.; funding acquisition, Y.T. All authors have read and agreed to the published version of the manuscript.

Funding: This research was funded by Natural Science project of Hunan Province, China, grant number 2020JJ5393 and Education Department of Hunan Province, China, grant number 21B0618.

Institutional Review Board Statement: Not applicable.

Informed Consent Statement: Not applicable.

Data Availability Statement: Not applicable.

Conflicts of Interest: The authors declare no conflict of interest.

Nomenclature

A	Cross section area [m ²]
C	Circumference [m]
C_p	Specific heat [J/kg-K]
d	Diameter [m]
f	Friction factor
G	Mass flux [kg/m ² -s]
h	Heat convection coefficient, [W/m ² -K]
k	Thermal conductivity [W/m-K], turbulent energy [J/kg]
L_p	Pitch length [m]
Nu	Nusselt number
P	Pressure [Pa]
Q	Heat flux [W/m ²]
Re	Reynolds number
T	Temperature [K]
u	Fluid velocity [m/s]
y	Wall distance [m]
ρ	Density [kg/m ³]
ΔP	Pressure drop [Pa]

Greek Symbols

α	Heat convection coefficient: [W/m ² -K]
ρ	Density [kg/m ³]
ω	Specific rate of turbulence dissipation [s ⁻¹]
μ	Dynamic viscosity [kg/m-s]
y	Wall distance [m]
θ	Bend angle [°]

Subscripts

b	Bulk
h	Hydraulic
in	Inlet
m	Pseudocritical point
out	Outlet
w	Wall

References

1. Chen, M.; Sun, X.; Christensen, R.N.; Shi, S.; Skavdahl, I.; Utgikar, V.; Sabharwall, P. Experimental and Numerical Study of a Printed Circuit Heat Exchanger. *Ann. Nucl. Energy* **2016**, *97*, 221–231. [[CrossRef](#)]
2. Kim, W.; Baik, Y.J.; Jeon, S.; Jeon, D.; Byon, C. A Mathematical Correlation for Predicting the Thermal Performance of Cross, Parallel, and Counterflow PCHes. *Int. J. Heat Mass Transf.* **2017**, *106*, 1294–1302. [[CrossRef](#)]
3. Pua, L.M.; Rumbold, S.O. Industrial Microchannel Devices—Where Are We Today? In *International Conference on Microchannels and Minichannels*; ASME: New York, NY, USA, 2003; Volume 1, pp. 773–780. [[CrossRef](#)]
4. Chen, M. Performance Testing and Modeling of Printed Circuit Heat Exchangers for Advanced Nuclear Reactor Applications. Ph.D. Thesis, University of Michigan, Ann Arbor, MI, USA, 2018.
5. Xu, X.Y.; Wang, Q.W.; Li, L.; Ekkad, S.V.; Ma, T. Thermal-Hydraulic Performance of Different Discontinuous Fins Used in a Printed Circuit Heat Exchanger for Supercritical CO₂. *Numer. Heat Transf. Part A Appl.* **2015**, *68*, 1067–1086. [[CrossRef](#)]
6. Nikitin, K.; Kato, Y.; Ngo, L. Printed Circuit Heat Exchanger Thermal-Hydraulic Performance in Supercritical CO₂ Experimental Loop. *Int. J. Refrig.* **2006**, *29*, 807–814. [[CrossRef](#)]
7. Kruiženga, A.; Anderson, M.; Fatima, R.; Corradini, M.; Towne, A.; Ranjan, D. Heat Transfer of Supercritical Carbon Dioxide in Printed Circuit Heat Exchanger Geometries. In Proceedings of the 14th International Heat Transfer Conference, IHTC 14, Washington, DC, USA, 8–13 August 2010; Volume 4, pp. 653–661. [[CrossRef](#)]
8. Saeed, M.; Kim, M.H. Thermal and Hydraulic Performance of SCO₂ PCHE with Different Fin Configurations. *Appl. Therm. Eng.* **2017**, *127*, 975–985. [[CrossRef](#)]
9. Douglas, A.; Olson, D.A. *Heat Transfer in Turbulent Supercritical Carbon Dioxide Flowing in a Heated Horizontal Tube*; NIST Pubs: Gaithersburg, MD, USA, 1998.
10. Tu, Y.; Zeng, Y. Heat Transfer and Hydraulic Characteristics of Supercritical CO₂ in Cooled and Heated Horizontal Semicircular Channels. *J. Appl. Fluid Mech.* **2021**, *14*, 1351–1362. [[CrossRef](#)]
11. Kim, D.E.; Kim, M.H.; Cha, J.E.; Kim, S.O. Numerical Investigation on Thermal-Hydraulic Performance of New Printed Circuit Heat Exchanger Model. *Nucl. Eng. Des.* **2008**, *238*, 3269–3276. [[CrossRef](#)]
12. Mohammed, H.A.; Gunnasegaran, P.; Shuaib, N.H. Influence of Channel Shape on the Thermal and Hydraulic Performance of Microchannel Heat Sink. *Int. Commun. Heat Mass Transf.* **2011**, *38*, 474–480. [[CrossRef](#)]
13. Matsuo, B.K.Y.; Ranjan, D.; Anderson, M. Numerical Study of Compact Heat Exchanger Designs for Generation IV Supercritical Carbon Dioxide Power Conversion Cycles. *Nucl. Sci. Eng.* **2014**, *176*, 138–153. [[CrossRef](#)]
14. Tsuzuki, N.; Kato, Y.; Ishiduka, T. High Performance Printed Circuit Heat Exchanger. *Appl. Therm. Eng.* **2007**, *27*, 1702–1707. [[CrossRef](#)]
15. Ngo, T.L.; Kato, Y.; Nikitin, K.; Ishizuka, T. Heat Transfer and Pressure Drop Correlations of Microchannel Heat Exchangers with S-Shaped and Zigzag Fins for Carbon Dioxide Cycles. *Exp. Therm. Fluid Sci.* **2007**, *32*, 560–570. [[CrossRef](#)]
16. Wen, Z.X.; Lv, Y.G.; Li, Q. Comparative Study on Flow and Heat Transfer Characteristics of Sinusoidal and Zigzag Channel Printed Circuit Heat Exchangers. *Sci. China Technol. Sci.* **2020**, *63*, 655–667. [[CrossRef](#)]
17. Dai, Z.; Zheng, Z.; Fletcher, D.F.; Haynes, B.S. Experimental Study of Transient Behaviour of Laminar Flow in Zigzag Semi-Circular Microchannels. *Exp. Therm. Fluid Science* **2015**, *68*, 644–651. [[CrossRef](#)]
18. Chen, M.; Sun, X.; Christensen, R.N. Thermal-Hydraulic Performance of Printed Circuit Heat Exchangers with Zigzag Flow Channels. *Int. J. Heat Mass Transf.* **2019**, *130*, 356–367. [[CrossRef](#)]
19. Yoon, S.J.; O'Brien, J.; Chen, M.; Sabharwall, P.; Sun, X. Development and Validation of Nusselt Number and Friction Factor Correlations for Laminar Flow in Semi-Circular Zigzag Channel of Printed Circuit Heat Exchanger. *Appl. Therm. Eng.* **2017**, *123*, 1327–1344. [[CrossRef](#)]
20. Ren, Z.; Zhao, C.R.; Jiang, P.X.; Bo, H.L. Investigation on Local Convection Heat Transfer of Supercritical CO₂ during Cooling in Horizontal Semicircular Channels of Printed Circuit Heat Exchanger. *Appl. Therm. Eng.* **2019**, *157*, 113697. [[CrossRef](#)]
21. Li, H.; Kruiženga, A.; Anderson, M.; Corradini, M.; Luo, Y.; Wang, H.; Li, H. Development of a New Forced Convection Heat Transfer Correlation for CO₂ in Both Heating and Cooling Modes at Supercritical Pressures. *Int. J. Therm. Sci.* **2011**, *50*, 2430–2442. [[CrossRef](#)]
22. Xiang, M.; Guo, J.; Huai, X.; Cui, X. Thermal Analysis of Supercritical Pressure CO₂ in Horizontal Tubes under Cooling Condition. *J. Supercrit. Fluids* **2017**, *130*, 389–398. [[CrossRef](#)]
23. Liu, S.; Huang, Y.; Wang, J. Theoretical and Numerical Investigation on the Fin Effectiveness and the Fin Efficiency of Printed Circuit Heat Exchanger with Straight Channels. *Int. J. Therm. Sci.* **2018**, *132*, 558–566. [[CrossRef](#)]
24. Tu, Y.; Zeng, Y. Flow and Heat Transfer Characteristics Study of Supercritical CO₂ in Horizontal Semicircular Channel for Cooling Process. *Case Stud. Therm. Eng.* **2020**, *21*, 100691. [[CrossRef](#)]
25. Batchelor, C.K.; Batchelor, G.K. *An Introduction to Fluid Dynamics*; Cambridge University Press: Cambridge, UK, 2000; ISBN 0521663962.
26. Kamiński, M.; Ossowski, R.L. Navier-Stokes problems with random coefficients by the Weighted Least Squares Technique Stochastic Finite Volume Method. *Arch. Civ. Mech. Eng.* **2014**, *14*, 745–756. [[CrossRef](#)]
27. Barth, T.J.; Jespersen, D.C. The Design and Application of Upwind Schemes on Unstructured Meshes. In *Aiaa Aerospace Sciences Meeting*; AIAA: Reston, VA, USA, 1989; p. 0366.

28. Li, H.; Zhang, Y.; Zhang, L.; Yao, M.; Kruiuzenga, A.; Anderson, M. PDF-Based Modeling on the Turbulent Convection Heat Transfer of Supercritical CO₂ in the Printed Circuit Heat Exchangers for the Supercritical CO₂ Brayton Cycle. *Int. J. Heat Mass Transf.* **2016**, *98*, 204–218. [[CrossRef](#)]
29. Kruiuzenga, A.; Li, H.; Anderson, M.; Corradini, M. Supercritical Carbon Dioxide Heat Transfer in Horizontal Semicircular Channels. *J. Heat Transf.* **2012**, *134*, 081802. [[CrossRef](#)]
30. Jackson, J.D. Fluid Flow and Convective Heat Transfer to Fluids at Supercritical Pressure. *Nucl. Eng. Des.* **2013**, *264*, 24–40. [[CrossRef](#)]
31. Dang, C.; Hihara, E. In-Tube Cooling Heat Transfer of Supercritical Carbon Dioxide. Part 2. Comparison of Numerical Calculation with Different Turbulence Models. *Int. J. Refrig.* **2004**, *27*, 748–760. [[CrossRef](#)]